Key Points:
- GNSS observations during August 2017 eclipse show total electron content (TEC) depletions up to 60% in magnitude
- Enhanced large-scale traveling ionospheric disturbances are observed before, during, and after totality
- Enhanced TEC is observed above Rocky Mountains 5-10 min after totality

Correspondence to:
A. J. Coster,
ajc@haystack.mit.edu

GNSS Observations of Ionospheric Variations During the 21 August 2017 Solar Eclipse

Anthea J. Coster[1] , **Larisa Goncharenko**[1] , **Shun-Rong Zhang**[1] , **Philip J. Erickson**[1] , **William Rideout**[1] , and **Juha Vierinen**[2]

[1] Haystack Observatory, Massachusetts Institute of Technology, Westford, MA, USA, [2] Department of Physics and Technology, University of Tromsø, Tromsø, Norway

Abstract On 21 August 2017, during daytime hours, a total solar eclipse with a narrow ~160 km wide umbral shadow occurred across the continental United States. Totality was observed from the Oregon coast at ~9:15 local standard time (LST) (17:20 UT) to the South Carolina coast at ~13:27 LST (18:47 UT). A dense network of Global Navigation Satellite Systems (GNSS) receivers was utilized to produce total electron content (TEC) and differential TEC. These data were analyzed for the latitudinal and longitudinal response of the TEC and for the presence of traveling ionospheric disturbances (TIDs) during eclipse passage. A significant TEC depletion, in some cases greater than 60%, was observed associated with the eclipse shadow, exceeding initial model predictions of 35%. Evidence of enhanced large-scale TID activity was detected over the United States prior to and following the large TEC depletion observed near the time of totality. Signatures of enhanced TEC structures were observed over the Rocky Mountain chain during the main period of TEC depletion.

Plain Language Summary On 21 August 2017, during daytime hours (16:00–20:00 UTC), a total solar eclipse was observed across the continental United States. A dense network of GPS receivers was utilized to monitor the changes in the ionosphere. GPS data were analyzed for the latitudinal and longitudinal response of the total electron content and for the presence of ionospheric perturbations during eclipse passage. A significant TEC depletion, in some cases greater than 60%, was observed associated with the eclipse shadow. Large-scale ionospheric perturbations were detected over the United States prior to and following the major TEC depletion observed near the time of totality. Signatures of enhanced TEC structures were also observed over the Rocky Mountain chain during the main period of TEC depletion.

1. Introduction

A total solar eclipse occurred over the continental United States on 21 August 2017, passing between coastlines in the 16:00–20:00 UT period. The 2017 eclipse had a characteristic shadow motion that remained supersonic during its transit, starting with speeds of ~3,600 km/h (~1,000 m/s) over Oregon and slowing to ~2,300 km/h (~ 650 m/s) over South Carolina. Solar eclipse effects on the ionosphere have been studied for more than 50 years, as they offer a naturally occurring "active" experiment with opportunities to study the effect of solar radiation on the ionosphere-thermosphere-mesosphere (ITM) system (Rishbeth, 1968). Recently, major advances in observational sensitivity and spatial/temporal resolution of radio-based techniques have provided new and more detailed information on the ITM response to eclipse forcing. In particular, eclipse studies for the 2017 event have benefited from the vast increase in fidelity and coverage of ground-based monitoring tools, especially Global Navigation Satellite Systems (GNSS) monitoring of total electron content (TEC).

This paper reports on early observational findings utilizing the GNSS data set for the 2017 August eclipse. Earlier research has shown that even in the partial shadow, the peak electron densities of the *F* and *E* ionospheric layers decreased by as much as 20–35% (Bamford, 2000). It is also predicted that the supersonic shadow of the Moon induces lower atmospheric acoustic and gravity waves that eventually reach ionospheric heights and generate traveling ionospheric disturbances (TIDs) (Chimonas, 1970; Chimonas & Hines, 1971). Comprehensive treatments of eclipse effects on the middle atmosphere, including studies of the differential

absorption of solar ultraviolet radiation by the ozone layer, have suggested that large-scale waves with periods of 2–4 h could be triggered by shadow passage (Fritts & Luo, 1993). TIDs with ∼20 min periodicity were first found in a beacon satellite TEC observation 1 h after totality passage (Davis & Rosa, 1970). Wave periods of eclipse-generated TIDs have been reported that vary from 4 min (Sauli et al., 2006) to 20–40 min (Ivanova et al., 1998), 60 min (Jakowski et al., 2008), and 87 min (Liu et al., 1998).

The work here relates to two major areas of the ITM response to solar eclipses. First, we present measurements of the intensity of the change in TEC and describe our initial analysis of the spatial and temporal difference between the main TEC depletion and that of the eclipse shadow moving across the United States. Note that as the eclipse shadow moves across the United States, it encounters the ionosphere at later solar times. As the shadow enters the United States over Oregon, the local time is near 10:00 LT, whereas when it exits over South Carolina, the local time is near 15:00 LT. Based on this observation, one would anticipate the largest ionospheric eclipse effects to be observed in the central part of the United States, between Wyoming and Missouri, when the local time is between noon and 13:00 LT.
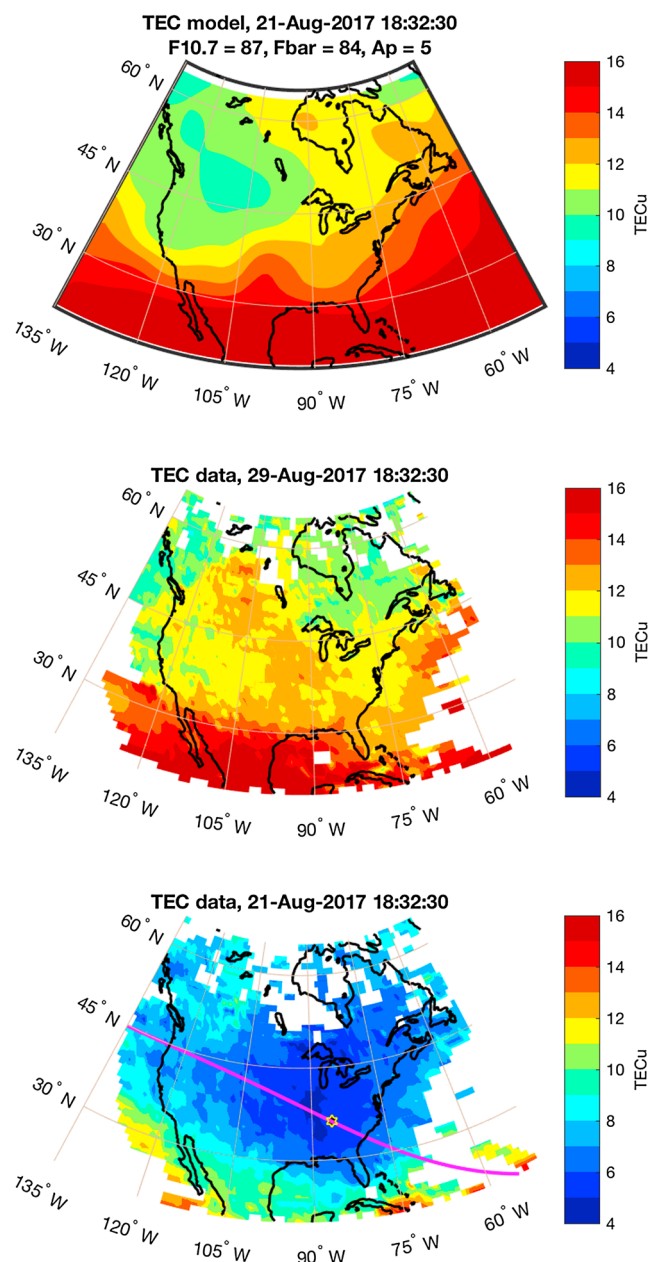
This paper's second focus area relates to traveling ionospheric disturbances (TIDs) associated with the eclipse shadow. An enhancement of large-scale TID (LSTID) activity is reported prior to, and following, the large TEC depletion associated with the eclipse. The observed LSTIDs propagate at speeds comparable to that of totality. In addition, approximately 10 min after totality, previously unreported signatures of TEC enhancements above the eastern and western sides of the Rocky Mountains are observed.

2. TEC Calculation and Perturbation Analysis

We utilize the worldwide network of GNSS receivers to monitor the ionospheric changes due to the solar eclipse. GNSS receivers have the advantage that they offer continuous high-resolution observations of the ionospheric TEC. MIT Haystack processes data from approximately 6,000 GPS geodetic receivers around the globe on a daily basis, corresponding to almost 100 million line-of-sight (LOS) TEC measurements. Approximately 2,000 GNSS receivers are located in North America. The GNSS processing algorithms used at Haystack were originally developed by Rideout and Coster (2006) and have been recently updated by Vierinen et al. (2015). For each satellite-receiver pair, the GNSS TEC has been converted to vertical TEC using the mapping function describe in Rideout and Coster (2006). TEC in this paper represents the vertical TEC directly above the location shown.

To isolate TEC changes induced by the eclipse, first, an empirical TEC model (NATEC, North America TEC) was employed to accurately separate the large-scale effects of the eclipse from ionospheric variations related to spatial, seasonal, and solar flux variations. The NATEC model was developed specifically for North America TEC (Chen et al., 2015) by applying an empirical orthogonal function (EOF) decomposition technique (Zhang et al., 2013) to TEC data measured from GNSS over the time period from 2001 to 2012. The model was demonstrated to well represent characteristic spatial variations over North America, especially for time periods of low geomagnetic disturbances. Chen et al. (2015) found a 1.2–2.6 TEC units (TECU; 1 TECU = 10^{16} el m^{-2}) mean average error of this model over NA for quiet geomagnetic time periods. TEC changes were also computed by differencing the measured TEC during the eclipse ($F_{10.7}$ = 87, Kp = 1–2) from measured TEC on 29 August 2017, the closest day with similar solar and geomagnetic activity ($F_{10.7}$ = 84, Kp = 1 − 2+). The $F_{10.7}$ flux values were obtained from Natural Resources Canada, and Kp values were obtained from GFZ German Research Center for Geosciences, Helmholtz Centre at Potsdam. As the 87 day mean $F_{10.7}$ value, $F_{10.7_{ave}}$, is not yet available as of this writing, an average flux of $F_{10.7}$ = 84 was used for the NATEC run as calculated from the data obtained before 18 September 2017.

Differential TEC values were computed for this study using a low-pass-filtering procedure based on the Savitzky-Golay low-pass filter (Savitzky & Golay, 1964). Differential TEC has been successfully used to observe both large-scale and medium-scale TIDs (Tsugawa et al., 2003, 2004). The filtering is done via a convolution process that utilizes a least squares fitting of successive subsets of adjacent TEC data points. The result is equivalent to detrending the data of each GNSS satellite-receiver pair with a fitted low-degree polynomial basis function. In this paper, we focus on results using a linear polynomial fitted over a 1 h interval. This filtering technique was selected to emphasize larger-scale perturbations in the ionosphere following the eclipse.

TEC model, 21-Aug-2017 18:32:30
F10.7 = 87, Fbar = 84, Ap = 5

TEC data, 29-Aug-2017 18:32:30

TEC data, 21-Aug-2017 18:32:30

Figure 1. Variation in TEC predicted by the (top) empirical TEC model over continental United States as expected on 21 August at 18:30 UT ($F_{10.7} = 87$, $F_{10.7_{ave}} = 84$, $Ap = 5$), (middle) observations from TEC receivers on 29 August 2017, non-eclipse day, and (bottom) observations from TEC receivers on 21 August 2017, eclipse day.

3. Results

3.1. Eclipse-Induced TEC Depletion

Figure 1 first plots the noneclipse state of the ionosphere using two different methods. Figure 1 (top) shows the variation in TEC predicted by NATEC over the continental United States on 21 August at 18:32 UT ($F_{10.7} = 87$, $F_{10.7_{ave}} = 84$, $Ap = 5$). The main features of the typical TEC model behavior are a gradual increase in TEC from the prenoon sector (9–11 TECU in the western area of the United States) to the afternoon sector (12–15 TECU in the eastern area of the United States) at midlatitudes, and higher TEC values at latitudes below $\sim$30°N (12–16 TECU). Figure 1 (middle) presents the TEC produced from the GNSS data and stored in the Madrigal database on 29 August 2017 ($F_{10.7} = 84$) and shows the same main features, although TEC values are slightly lower than expected from NATEC for $F_{10.7} = 87$.

Figure 1 (bottom) presents TEC observations at 18:32 UT on the day of solar eclipse. The path of totality is shown with a magenta line, and the hexagon symbol indicates the center of totality at 18:32 UT. On the eclipse day, a much lower TEC was observed over the entire area of the continental United States. The area of lowest TEC, 4–5 TECU, is located at 90°W, several degrees to the west of the center of totality, indicating that the largest impact of solar eclipse on ionospheric electron density occurs several minutes after the totality. For reference, the geomagnetic north latitude at the hexagon symbol is 46.8°, at the entry along the west coast it is 50.31°, and at the exit along the east coast it is 42.11°.

Figure 2 presents the estimated TEC changes produced by differencing the TEC measured during the eclipse from the NATEC model predicted TEC (left column) and from the 29 August 2017 TEC observations (right column). Figure 2 (top row) shows the difference in absolute TEC units, while Figure 2 (bottom row) shows the relative difference expressed as a percentage of the background. Changes in TEC are remarkably similar, regardless of the background TEC calculation method. The maximum decrease in TEC reaches 6–8 TECU (50–60% of the expected background level) in the vicinity of the eclipse shadow zone. The area of 50% decrease is extended approximately 15° in longitude ($\sim$1,500 km) to the west from the center of totality and $\sim$7–10° in longitude to the east, and the area of $\sim$30% decrease in TEC is extended $\sim$30° to the west of the totality. The western United States shows the beginning of the recovery to expected TEC values, though the ionosphere is still depleted by 10–20%. Notably, the area of the decrease in TEC is not symmetric in latitude and is extended from the totality path to the south, covering Florida and Central America, as seen in Figure 2 (top left). More details on the complex time evolution of the eclipse-induced disturbance zone are under study and will be reported in a separate publication.

Since the state of the ionosphere is directly related to the ionizing solar radiation, the decrease in solar radiation due to the passage of lunar shadow is expected to result in the decrease of ionospheric electron density. However, the ionospheric response to any particular eclipse can vary widely depending on the solar activity, season, and latitude, with reported decreases ranging from 15% drop in TEC at midlatitudes (Bamford, 2000) to 30–58% at low latitudes (Kumar & Singh, 2012). At middle latitudes the depletion of total electron content (TEC) during a total eclipse is about 30–40% (e.g., Jakowski et al., 2008; Krankowski et al., 2008). We emphasize that we cannot attribute the entire >60% decrease in TEC purely to solar eclipse processes, as the ionosphere can experience variations of 1–2.5 TECU on a daily basis. Both positive and negative differences (of the order of 1–2.5 TECU) were observed between 75 and 95°W longitude prior to the start of the eclipse on 21 August when compared to the control day on 29 August 2017 (not shown here). Although the 30 h prior to the eclipse were relatively quiet ($Kp = 3$ or less), some of the observed differences in TEC can be partially attributed to the moderate geomagnetic activity that occurred early in the day on
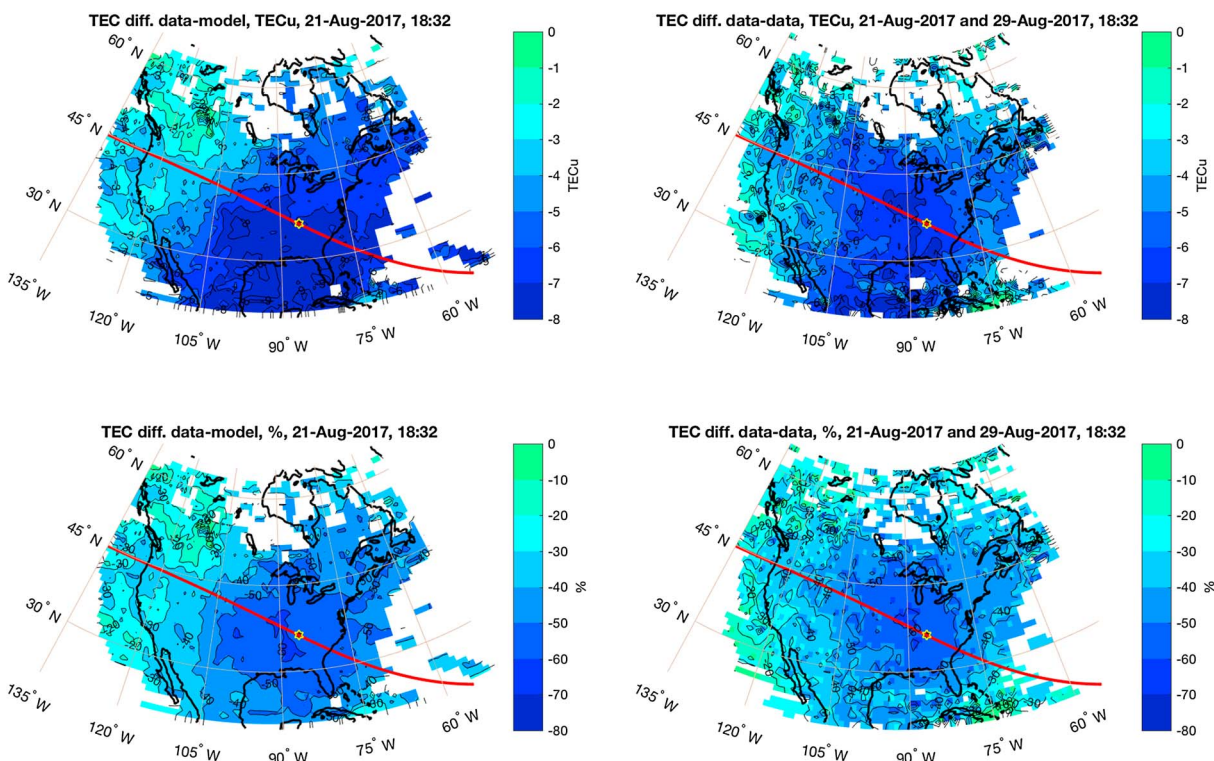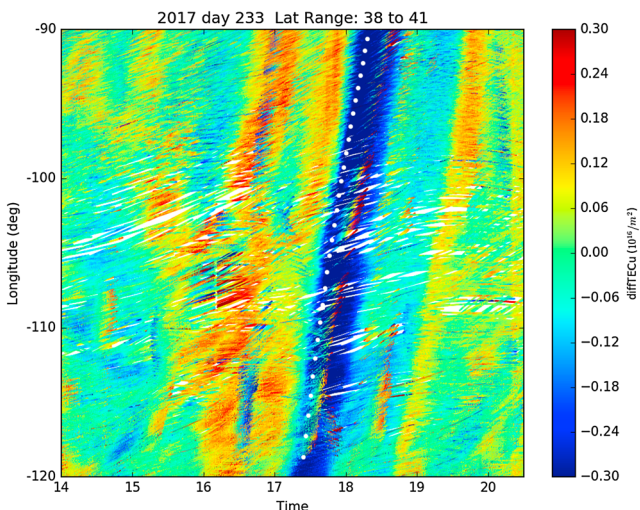
Figure 2. Difference in TEC (left column) between TEC observations during the solar eclipse and NATEC predictions, and (right column) between TEC observations on 21 August 2017 (eclipse day) and 29 August 2017 (non-eclipse day). Figure 2 (top row) shows absolute difference in TECU and (bottom row) shows the difference expressed as percentage of background TEC.

20 August ($Kp = 5$ between 0 and 6 UT) and for several days prior to 21 August. After the start of partial eclipse (1.5 h prior to totality), a decrease in TEC is the dominant response.

The TEC decrease during the 21 August 2017 eclipse is somewhat larger than the ~5 TECU (35%) predicted by the SAMI3 simulations of Huba and Drob (2017). The daytime level of TEC for the noneclipse case is in good agreement between NATEC and SAMI3, at least for ~90°W longitude and 16–19 UT (not shown here). According to NATEC estimates, the difference between the solar flux conditions used in the Huba and Drob (2017) simulation ($F_{10.7} = 90$, $F_{10.7_{ave}} = 90$, $Ap = 4$) and actual conditions account for a 0.9–1.1 TECU difference at middle latitudes and 1.5 TECU difference below 30°N. The Huba and Drob (2017) study utilizes SAMI3, a first principles ionosphere/thermosphere model. Their study did not include the response of the thermosphere to the solar eclipse nor its subsequent impact on the ionosphere. The differences between their simulations and our observations suggest that eclipse-induced changes in the thermosphere did indeed occur and that these changes involve the temperature, thermospheric wind, and composition. Our results suggest that these factors play an important role in the overall ionospheric modification during the solar eclipse.

3.2. Eclipse-Induced Ionospheric Disturbances

Figure 3. Keogram of LSTIDs characteristics seen at 40°N latitude. The white dotted line shows the longitude location of the eclipse totality.

Figure 3 presents a keogram image of differential TEC derived using the perturbation analysis technique described earlier. In this keogram, differential TEC values were averaged over the latitude range of 38°N to 41°N and are shown as a function of longitude and time. The majority of the motion of the 2017 solar eclipse across the United States was in longitude, rather than latitude. The horizontal axis shows 14:00 UT to 20:30 UT, a time period that spans the entirety of when the eclipse penumbra could be observed over the continental United States. The penumbra is the partially shaded outer region of the shadow cast by the eclipse, and it first touched the Oregon coast

at 16:00 UT. At its maximum during the 2017 eclipse, the penumbra had a radius of 7,500 km, covering all of CONUS. In contrast, the umbra, or region of totality, has a radius of approximately 160 km. The white dots shown in Figure 3 indicate the longitude and time location of totality. The average speed derived from the keogram provides a reasonable estimate of the zonal speed of totality. At 17:30 UT, the measured speed of totality was 920 m/s, of which 910 m/s was observed in the zonal component and −146 m/s was the meridional component. This speed will vary as a function of time as the speed of totality was not constant across the United States.

In the center of Figure 3's keogram, a large blue feature extends from −120° to −90° longitude and has a width of approximately 30–40 min. This corresponds to the TEC depletion associated with the eclipse. The speed of this feature across the United States is 850–1,000 m/s, consistent with the speed of totality. Note that some of this depletion is observed prior to totality and that the largest depletion is observed ∼10 min after totality. This is consistent with the 22 July 2009 eclipse observations reported by Ding et al. (2010) of a TEC depletion area with a maximum decrease of 5 TEC that moved eastward following the movement of totality with a response time lag of ∼10 min. The observed features of the TEC depletion are also in agreement with those discussed by Jakowski et al. (1999, 2001). What should be noted is that the TEC depletion is not uniform across the keogram and that this keogram does not show the latitude dependency of totality. Different ionospheric behavior is anticipated at different latitudes based on previous studies (Jakowski et al., 2008; Le et al., 2009). A separate study is underway to examine further details of this effect.

Figure 3 also highlights two other types of TEC perturbations associated with the eclipse. First, both before and after the eclipse, additional large-scale TIDs can be observed propagating at a similar speed to that of the eclipse shadow across the United States. As observed in Figure 3, prior to 16:00 UT, TID activity is small. A clear enhancement in TID activity begins around 16:00 UT when the penumbra shadow first reaches Oregon. Immediately after 16:00 UT, a feature is observed that begins at −120° longitude and has a width of ∼30 min. Following this, a second feature is observed that begins at 16:40 UT and −118° longitude with a width of ∼15 min. Later, following the primary eclipse TEC depletion, two other large TID features are observed. The first, which begins at approximately 18:00 UT, has a width of ∼60 min and is negative. The second begins at 18:45 UT, has a width of ∼15 min, and is positive. The last feature is likely related to the penumbra finally exiting the continental United States.

We note that geomagnetic activity was low on 21 August 2017 with a maximum Kp of 3, and during the solar eclipse hours of 15:00–21:00 UT, Kp remained between 1 and 2. Clearly, the fast-moving LSTIDs moving to the east are not associated with geomagnetic activity. Preeclipse TIDs traveling at 150 m/s in the zonal direction were visible in an earlier time period of the keogram (not shown) with fundamentally different signatures from the LSTIDs seen near the eclipse period. The eclipse LSTIDs that could be originated in situ within the thermosphere and simulations by Muller-Wodarg et al. (1998) have suggested this possibility, but this zonal propagation at a very large speed of 800–900 m/s is still somewhat unexpected, although it appears to agree with results shown in Figure 2 of Muller-Wodarg et al. (1998).

Previous studies indicated that the supersonic moving moon shadow should produce TIDs of variable size, depending on the distance from the totality zone, due to gravity wave excitation in the middle atmosphere (Chimonas, 1970; Chimonas & Hines, 1971). Jakowski et al. (2008) reported that during the October 2005 eclipse enhanced wave activity was observed with ionosonde and HF Doppler measurements, but not with TEC data analysis. They suggested that the wave amplitudes were too small to be detected via the interpolation method they used for GNSS processing. The GNSS analysis technique used in the current study utilizes more ground-based sensors and is more sensitive to changes. For the 2017 eclipse, our TID observations with the 1 h sliding window and linear basis function also reveal bow-shaped TIDs, and a further analysis using a 30 min window provides very clear views of the bow waves. This will be reported in a separate study.

The second type of TID phenomenon that can be observed in Figure 3 is the positive TID structure in the center of the primary TEC depleted region. This feature is first observed at ∼17:30 UT and propagates at speeds comparable to that of the umbra (∼900 m/s). It is clearly visible from −108° to −100° longitude, intensifying between −106° and −100° longitude.

Figure 4 further illustrates the enhanced TEC structure that is observed within the primary TEC depleted region. In Figure 4 (top), a feature occurs at 17:32 UT that extends along the western edge of the Rocky Mountain range (scale = [−0.1, 0.1] TECU). The magenta triangles on the map represent McBride, CA (latitude = 53.30,
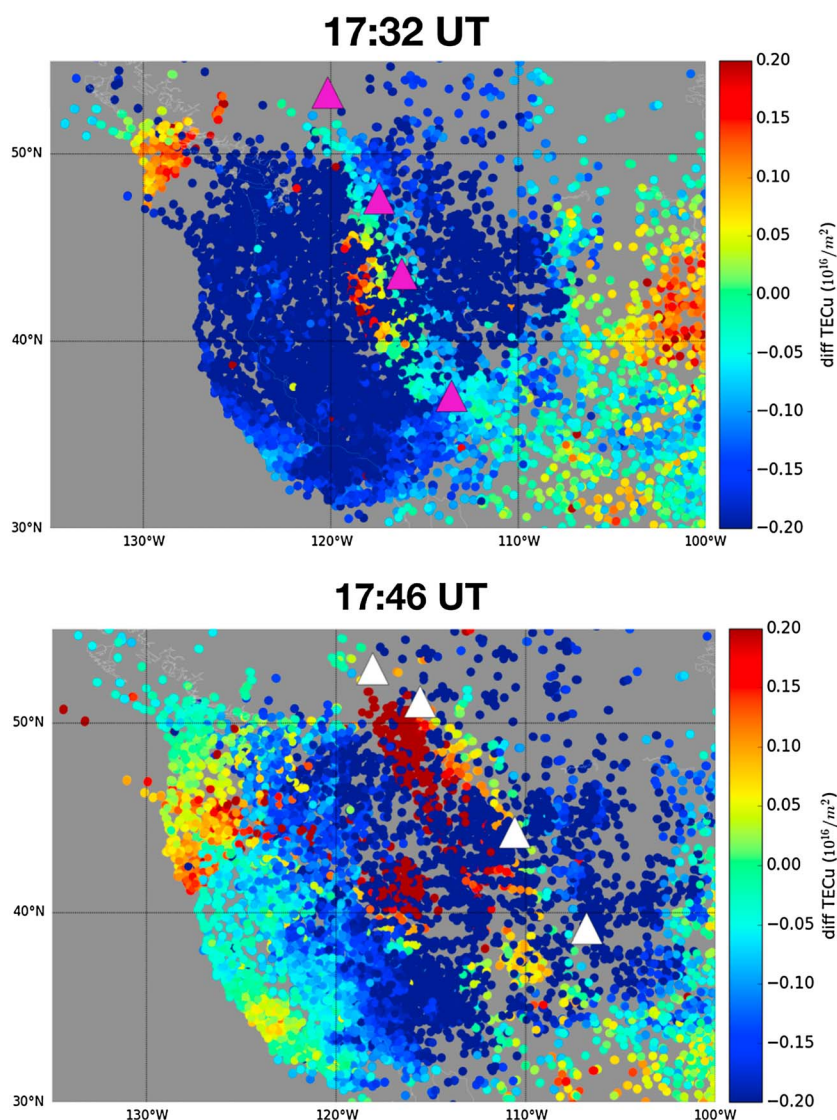
Figure 4. Evidence of enhanced TID on the western side and eastern side of the Rocky Mountain range. (top) The magenta triangles represent McBride, CA; Spokane, WA; Boise, ID; and St. George, UT; (bottom) the white triangles represent Jasper, CA; Banff, CA; Jackson, WY; and Aspen, CO.

longitude = −120.17); Spokane, WA (latitude = 47.66, longitude = −117.43); Boise, ID (latitude = 43.62, longitude = −116.21; and St. George, UT (latitude = 37.10, longitude = −113.57). The latitudes and longitudes given are all in geographic coordinates. The umbra passes close to Boise, ID, at 17:28 UT, although effects of the shadow were observed at Boise as early as 17:20 UT. Figure 4 (bottom) shows a similar enhanced TEC feature at 17:48 UT above the eastern side of the Rocky Mountains, where the white triangles represent Jasper, CA (latitude = 52.87, longitude = −118.08); Banff, CA (latitude = 51.17, longitude = −115.57); Jackson, WY (latitude = 44.26, longitude = −110.60); and Aspen, CO (latitude = 39.19, longitude = −106.82). The umbra passed over Jackson, WY, at 17:36 UT. This enhanced TEC feature was observed to propagate from west to east and appears larger on the eastern coast of the Rockies. Other wave-like features can also be detected, including the appearance of structures, primarily propagating in the meridional direction, that appear to be propagating outward from the large depletion area.

We suggest that this TEC enhancement over the Rocky Mountains is caused by processes triggered by the eclipse, perhaps due to large temperature changes on the ground that induced or enhanced locally produced atmospheric waves in the mountain region. Large changes in mesosphere-lower thermosphere (MLT) zonal winds during eclipses have been observed by Ramkumar et al. (2013). They observed a reversal of zonal winds

at 98 km during the maximum phase of the January 2010 eclipse at local noon. They attributed this change in the winds to eclipse-induced cooling and pressure changes in the middle atmosphere. Separately, Smith et al. (2009) reported on observations of stationary mesospheric gravity waves observed over the Andes during July 2008 (local winter) at the El Leoncito Observatory in Argentina. Mountain waves are not typically observed in the summer months. Smith et al. (2009) postulated that these waves were mountain waves generated by a 70 m/s eastward wind flowing over the Andes. Vertically propagating mountain waves may have horizontal wavelengths of many tens of kilometers or more and usually extend upward into the lower stratosphere and are often standing or nearly standing waves. The band-like structures that Smith et al. (2009) observed had a near-zero horizontal phase speed and were aligned parallel with the Andes. Bacmeister et al. (2012) analyzed an event in Norway due to a temperature perturbation of over 5 K, concluding that mountains can play a significant role in producing small-scale and medium-scale variability in the lower stratosphere. For the eclipse scenario, a possible generator for the excitation of orographic-related gravity waves and TEC enhancement are the known temperature changes. The National Weather Service reported a 6.1°C change in temperature over Douglas, WY, as a consequence of the eclipse, with 3.9°C occurring in the last 20 min of the umbra's passing and the minimum temperature delayed by 5 min after totality. The temperature then reversed itself increasing 3.9°C over the following 20 min.

In Figure 4, the observed TEC enhancement over the Rocky Mountains appears to follow totality, which suggests high propagation speed, greater than 750 m/s. This speed is much higher than anticipated speeds of 250–350 m/s for gravity waves. One possibility is that we are observing standing waves, similar to those in the study of Smith et al. (2009), that are excited at each point along the totality passage over the mountains. Once the umbra has passed and the temperature begins to increase, these waves decay.

4. Summary

On 21 August 2017, during daytime hours (16:00–20:00 UTC), a total solar eclipse moved across the continental United States along a path from Oregon to South Carolina with a narrow ~160 km wide umbral shadow. Outside of this region, a partial solar eclipse associated with the penumbra covered the majority of the continental United States. GNSS data during eclipse passage were analyzed to study the latitudinal and longitudinal response of the TEC changes and to observe the presence of TIDs.

Both methods of background removal showed a significant TEC depletion associated with the eclipse shadow, in some cases greater than 60%, exceeding initial model predictions (Huba & Drob, 2017). The resulting analysis showed a continental scale reduction of TEC, with the peak reduction trailing the totality path by approximately 10 min. The differences observed between the measured TEC response and the initial model predictions (Huba & Drob, 2017) are likely due to thermospheric changes in the neutral wind, temperature, and the N_2 and O densities not being accounted for in the initial simulation.

The TID analysis discussed in this paper was tailored for studies of large-scale TIDs. Associated with totality, a strong TEC depletion was observed to move across the United States at speeds comparable to that of the eclipse. Prior to and following this large TEC depletion, enhanced large-scale TIDs were observed over the United States. The speed of these LSTIDs (850 m–1,000 m/s) was comparable to the speed of the eclipse. The initial TID observations were positive (enhanced TEC) and could be related to a large-scale bow shape disturbance in front of the penumbra of the eclipse. Signatures of enhanced TEC structure are also observed over the Rocky Mountain chain during the main period of TEC depletion. Although not well understood, the interaction of eclipse-induced mountain waves due to surface changes in pressure and temperature coupled with the eclipse-induced ozone cooling and other wind variations may produce the observed enhanced TEC over the Rockies.

References

Bacmeister, J. T., Schoeberl, M. R., Lait, L. R., Newman, P. A., & Gary, B. (2012). Small-scale waves encountered during AASE. *Geophysical Research Letters*, *17*, 349–352. https://doi.org/10.1029/GL017i004p00349

Bamford, R. A. (2000). The effect of the 1999 total solar eclipse on the ionosphere. *Physics and Chemistry of the Earth (C)*, *26*(5), 373–377, 2001.

Chen, Z., Zhang, S.-R., Coster, A. J., & Fang, G. (2015). EOF analysis and modeling of GPS TEC climatology over North America. *Journal of Geophysical Research: Space Physics*, *120*, 3118–3129. https://doi.org/10.1002/2014JA020837

Chimonas, G. (1970). Internal gravity-wave motions induced in the Earth's atmosphere by a solar eclipse. *Journal of Geophysical Research*, *75*(28), 5545–5551.

Chimonas, G., & Hines, C. O. (1971). Atmospheric gravity waves induced by a solar eclipse, 2. *Journal of Geophysical Research*, *76*(28), 7003–7005.

Davis, M. J., & Rosa, A. V. D. (1970). Possible detection of atmospheric gravity waves generated by the solar eclipse. *Nature*, *226*(5251), 1123–1123.

Ding, F., Wan, W., Ning, B., Liu, L., Le, H., Xu, G., . . . Yang, M. (2010). GPS TEC response to the 22 July 2009 total solar eclipse in East Asia. *Journal of Geophysical Research*, *2010*, A07308. https://doi.org/10.1029/2009JA015113

Fritts, D. C., & Luo, Z. (1993). Gravity wave forcing in the middle atmosphere due to reduced ozone heating during a solar eclipse. *Journal of Geophysical Research*, *98*(D2), 3011–3021.

Huba, J. D., & Drob, D. (2017). SAMI3 prediction of the impact of the 21 August 2017 total solar eclipse on the ionosphere/plasmasphere system. *Geophysical Research Letters*, *44*, 5928–5935. https://doi.org/10.1002/2017GL073549

Ivanova, V. A., Ryabova, N. V., & Shumaev, V. V. (1998). Effect of the solar eclipse of 22 July 1990 at mid-latitude path of HF propagation. *Journal of Atmospheric and Solar Terrestrial Physics*, *59*, 1013–1016.

Jakowski, N., Heise, S., Wehrenpfennig, A., & Schlueter, S. (2001). Total electron content studies of the solar eclipse on 11 August 1999. CD-ROM, Proc. IBSS, Boston, MA 4-6 June, 2001, 279–283.

Jakowski, N., Schlueter, S., Heise, S., & Feltens, J. (1999). Satellite technology glimpses ionospheric response to solar eclipse. *EOS Transactions American Geophysical Union*, *80*(51), 621–626.

Jakowski, N., Stankov, S. M., Wilken, V., Borries, C., Altadill, D., Chum, J., . . . Canderd, L. R. (2008). Ionospheric behavior over Europe during the solar eclipse of 3 October 2005. *Journal of Atmospheric and Solar-Terrestrial Physics*, *70*(6), 836–853.

Krankowski, A., Shagimuratov, I. I., Baran, L. W., & Yakimova, G. A. (2008). The effect of total solar eclipse of October 3, 2005, on the total electron content over Europe. *Advances in Space Research*, *41*(4), 628–638.

Kumar, S., & Singh, A. K. (2012). Changes in total electron content (TEC) during the annular solar eclipse of 15 January 2010. *Advances in Space Research*, *49*(1), 75–82.

Le, H., Liu, L., Yue, X., Wan, W., & Ning, B. (2009). Latitudinal dependence of the ionospheric response to solar eclipses. *Journal of Geophysical Research*, *114*, A07308. https://doi.org/10.1029/2009JA014072

Liu, J. Y., Hsiao, C. C., Tsai, L. C., Liu, C. H., & Kuo, F. S. (1998). Vertical phase and group velocities of internal gravity waves derived from ionograms during the solar eclipse of 24 October 1995. *Journal of Atmospheric and Solar Terrestrial Physics*, *60*(1998), 1679–1686.

Muller-Wodarg, I. C. F., Aylward, A. D., & Lockwood, M. (1998). Effects of a mid-latitude solar eclipse on the thermosphere and ionosphere—A modelling study. *Geophysical Research Letters*, *25*(20), 3787–3790.

Rideout, W., & Coster, A. (2006). Automated GPS processing for global total electron content data. *GPS Solutions*, *10*(3), 219–228. https://doi.org/10.1007/s10291-006-0029-5

Rishbeth, H. (1968). Solar eclipses and ionospheric theory. *Space Science Reviews*, *8*, 543–554.

Ramkumar, G., Subrahmanyam, K. V., Kishore Kumar, K., Das, S. S., Swain, D., Sunilkumar, S. V., . . . Babu, A. (2013). First observational study during a solar eclipse event on variations in the horizontal winds simultaneously in the troposphere-stratosphere-mesosphere-lower-thermosphere region over the equatorial station Thumba (8.5°N, 77°E). *Earth Planets Space*, *65*, 781–790.

Sauli, P., Abry, P., Boska, J., & Duchayne, L. (2006). Wavelet characterisation of ionospheric acoustic and gravity waves occurring during the solar eclipse of August 11, 1999. *Journal of Atmospheric and Solar-Terrestrial Physics*, *68*(3), 586–598.

Savitzky, A., & Golay, M. J. E. (1964). Smoothing and differentiation of data by simplified least squares procedures. *Analytical Chemistry*, *36*, 1627–1639.

Tsugawa, T., Saito, A., & Otsuka, Y. (2004). A statistical study of large-scale traveling ionospheric disturbances using the GPS network in Japan. *Journal of Geophysical Research*, *109*, A06302. https://doi.org/10.1029/2003JA010302

Tsugawa, T., Saito, A., Otsuka, Y., & Yamamoto, M. (2003). Damping of large-scale traveling ionospheric disturbances detected with GPS networks during the geomagnetic storm. *Journal of Geophysical Research*, *108*(A3), 1127. https://doi.org/10.1029/2002JA009433

Smith, S., Baumgardner, J., & Mendillo, M. (2009). Evidence of mesospheric gravity waves generated by orographic forcing in the troposphere. *Geophysical Research Letters*, *36*, D21103. https://doi.org/10.1063/1.3069210

Zhang, S.-R., Chen, Z., Coster, A. J., Erickson, P. J., & Foster, J. C. (2013). Ionospheric symmetry caused by geomagnetic declination over North America. *Geophysical Research Letters*, *40*, 5350–5354. https://doi.org/10.1002/2013GL057933

Vierinen, J., Coster, A. J., Rideout, W. C., Erickson, P. J., & Norberg, J. (2015). Statistical framework for estimating GNSS bias. *Atmospheric Measurement Techniques Discussions*, *8*(9), 9373–9398. https://doi.org/10.5194/amt-9-1303-2016